Geophysical Research Letters

Supporting Information for

A 15-year slow slip event on the Sunda megathrust off Sumatra

Louisa L. H. Tsang[1], Aron J. Meltzner[1], Belle Philibosian[2], Emma M. Hill[1], Jeffrey T. Freymueller[3] and Kerry Sieh[1]

[1] Earth Observatory of Singapore, Nanyang Technological University, Singapore

[2] Tectonics Observatory, California Institute of Technology, California, U.S.A (now at Columbia University, New York, U.S.A)

[3] University of Alaska Fairbanks, Alaska, U.S.A

Contents of this file

Additional Supporting Information

Introduction

This supplementary information contains additional details of the coral data and the modeling methods for the various scenarios that we present in the paper. We include sketches of the coral slabs and time series at each of the sites in our study area (Figures S1 to S6; displacement rates are also listed in Table S1). We provide complete details of our analysis of the Aviso data and calculation of additional rate uncertainties due to spatial variations in sea level (Text S1, Table S2). We also present our analysis of the time series of mean SLA and SLA rates from the Aviso data in Text S1, Figures S8 and S9. A discussion of corrections for modern sea-level rise can be found in Text S2. We provide further details of our fault geometry and justification of our modeling assumptions (Text S4, Figures S7 and S10), alternative backslip and SSE models (Figures S12, Tables S3 to S5), and sensitivity tests of our models (Figures S11 and S13). Methods and results of our inversion models can be found in Text S3 and Figure S14. Table S6 lists the subduction zone slow slip events that are plotted in Figure 3.

Text S1.

Investigating local differences in sea level due to oceanographic processes

An intriguing observation of our coral dataset is the spatial variation of the rate changes: rates at sites in the Banyak Islands changed around 1966 and 1981, but significant changes are not observed at these times on southern Simeulue or northern Nias. Because rates of RSL change reflect changes both in land level and in absolute sea level, it is important to consider how much of this could result from changes in local sea level.

The 2σ (95%) level uncertainties listed in Table S1 were determined following the methodology of *Meltzner et al.* [2012, 2015] and consider uncertainties in the calculated rates that may arise from coral irregularities, but not from variability in sea level itself. At a single site, individual coral microatolls may have experienced differential erosion rates, or may have contrasting morphologies due to differential growth rates. These two physical factors lead to potential irregularities in a single coral colony that could bias its RSL history. *Meltzner et al.* [2012] addressed this issue by comparing RSL histories of coeval coral microatolls at a particular site, and they determined the maximum difference in the HLG (highest level of growth) between corals, within any year. They found a worst-case scenario error of 80 mm (which they conservatively treated as an error at the 95% confidence level) in the apparent elevation gain of a single coral colony due to differential erosion and growth rates. Based on these observations, *Meltzner et al.* [2012] suggested a formal method to calculate the 2σ error in the rates of RSL change determined from coral microatolls off the west coast of Sumatra: this worst-case scenario error (80 mm) is divided by the length of time over which each coral displacement rate was determined.

We also wish to consider the extent to which spatial variations in the coral vertical displacement rates can be explained by spatial variations in sea level. In a manner parallel to that of *Meltzner et al.* [2012], we considered the difference between the elevation gains recorded by corals at two sites over a particular time interval, and we desired to estimate, at the 95% confidence level, how much of that difference could be attributable to differences in absolute sea level at the two sites.

For this purpose, we analyzed modern satellite altimetry data to quantify spatial variations of sea level in the Simeulue-Nias region. We selected the delayed-time mode, all-satellite merged product of globally gridded sea level anomalies (SLAs), produced by Ssalto/DUACS, and distributed by Aviso (www.aviso.altimetry.fr/duacs). The data span January 1993 to April 2014, and consist of daily SLAs estimated on a global grid, at a spatial resolution of 0.25° by 0.25°. We first extracted the time series of daily SLAs at 25 grid points in a 1.25° by 1.25° region centered between Simeulue and Nias (Figure S8a). In order to smooth out unmodeled high frequency ocean signals and aliasing effects in the data, we estimated the mean SLA for each day with a ± 30 day running time window, to obtain time series of 2-month mean SLAs at daily resolution (Figure S8b). In principle, this reduces the contribution of aliased signals with periods less than 2 months [*Ponte et al.*, 2002]. Next, we calculated the difference in the SLA between each pair of grid points—for example, grid point 1 was differenced with each of the remaining 24 grid points (Figure S8c). We then determined the 95th percentile of mean SLA differences between grid points. Figure S8d shows the cumulative frequency

histogram of mean SLA differences between grid points, and the values containing 65 and 95 percent (65th and 95th percentile) of the data. The 95th percentile of mean SLA differences is 17.3 mm. We caution that near-coastal shallow-water areas can have deviations from deeper-water open-ocean sea levels that are not captured by AVISO's gridded product, but these deviations are not well understood or modeled. Nonetheless, most of our sites (PBK, PUB, SBA, MZL, and LBJ) are within 3 km of water that is 20 m deep or deeper, and they are within 10 km of 50-m-deep water. PLM is in a somewhat shallower setting, being 7 km from the 20-m bathymetric contour, and 11 km from 50-m water depths.

We treated the magnitude of these spatial variations in SLAs as an independent error and added this error in quadrature to the uncertainties due to potential coral irregularities that we previously calculated following *Meltzner et al.* [2012]. These modified errors are given in Table S2. Our hypothesis is that if the summed uncertainties in the displacement rate changes at each site do not overlap at the 1σ confidence level, then the spatiotemporal changes in the coral displacement rates are unlikely due to oceanographic sea-level changes, and more likely consistent with tectonic changes on the underlying megathrust.

As we can see in Table S2, considering both sources of error, the rate change at PBK around 1966 was +10.6 ± 4.5 mm/yr (2σ). This differs significantly from the permissible rate change at site LBJ, 0.0 ± 2.2 mm/yr. The rate change at PLM is not well constrained, but if only 1σ errors are considered, it does not overlap the rate change at PBK. In 1981, the rate change at PBK, −10.2 ± 2.7 mm/yr (2σ), differs significantly from the permissible rate changes at sites LBJ, SBA, and MZL. Again, the rate changes at PLM and PUB are not well determined, but if only 1σ errors are considered, neither overlaps the rate change at PBK.

Investigating spatiotemporal changes in SLA rates

We also sought to understand the spatiotemporal changes in SLA rate in our study area. The same globally gridded SLA dataset was used. For each grid point in our study area, we computed the time series of SLA rates. In order to smooth out the contribution of seasonal and interannual oceanographic signals, we computed the daily SLA rates with a running time window of ± 8 years. This length of time window averages out interannual sea surface signals with periods of less than ~ 16 years. To illustrate the sensitivity of the results to the time window length, we have presented in Figure S9 the results of using time windows ranging from ± 5 to ± 10 years. Because we do not fully understand the seasonal and interannual oceanographic processes in this region, we caution against detailed interpretation of these time series of SLA rates. Furthermore, due to the spatial resolution of the dataset (and spatial interpolation), local coastal effects may not be captured in the Aviso data. Understanding such local processes awaits data from regional tide gauges or future satellite missions. Therefore, the objective of this analysis was to show only to first order the spatial differences in sea-level trends across this region.

Figure S9a shows the time series of SLA rates estimated with a ± 8-year running time window, for each grid point. Similar time series for all grid points suggests that the whole region experiences coherent sea-level changes with time. To validate this, we calculated the differences in the time series of SLA rates between grid points, to quantify the spatial differences in sea-level trends across this region. It should be noted that these differences are sensitive to the length of running time window chosen. We calculated the time series of SLA

rate differences between each pair of grid points - for example, grid point 1 is differenced with each of the remaining 24 grid points. The results are shown in Figure S9b.

The 95% confidence level of SLA rate differences is 0.9 mm/yr. This magnitude of difference is much less than the magnitude of rate changes between any two time periods (e.g. between 1966 – 1981, and 1981 – 2005), shown in Table S2. With a shorter running time window of ± 5 years, the results suggest an SLA rate difference of 1.4 mm/yr at the 95% confidence level, which is still less than the magnitude of rate changes between any two time periods.

Text S2.

Corrections for long-term sea-level rise

Following the methodology of *Meltzner et al.* [2010], the RSL time series at each coral site were adjusted vertically by a constant 2 mm/yr, to account for eustatic sea-level rise in the 20th century. This correction compares well with average estimates of sea-level rise in the Indian Ocean from ~ 1945 to 2007, from previous studies of 20th century sea-level rise [*Beckley et al.,* 2007; *Hamlington et al.,* 2011; *Jevrejeva et al*., 2006]. However, these studies also show that rates of sea-level rise vary with time, within a given region. For example, *Jevrejeva et al*. [2006] estimated variable rates of sea level rise in the Indian Ocean during different time periods: between 1938 to 2000, rates of sea-level rise decreased non-linearly from ~ + 3.9 to ~ + 0.2 mm/yr. Specifically, the rate of sea-level rise between ~1930 and 1947 was ~ + 4 mm/yr; between ~1947 and 1958 the rate was ~ + 3 mm/yr; between 1958 and 1965, ~ +2 mm/yr; between 1965 and 1980, ~ + 1 mm/yr; and from 1980, ~ +0.2 mm/yr.

By analyzing tide gauge data from ~1900, some researchers have reported 60-year oscillations in global sea level, which suggest a fall in mean sea level after 1960 [*Chambers et al*., 2012; *Woodworth et al*., 2009]. These oscillations were assumed or argued by the respective authors to operate on the scale of entire ocean basins, leading us to expect contemporaneous changes in RSL at all sites within our study region. However, the coral data show that while sites in the Banyak Islands experienced significant RSL change from 1966-1981, similar changes are precluded at sites on the neighboring islands of Simeulue and Nias. Hence, if multi-decadal fluctuations in sea level are responsible for the coral observations in the Banyak Islands, these sea-level fluctuations must have been extremely limited in geographic extent, and they must have been distinct from the basin-wide oscillations suggested by *Woodworth et al*. [2009] and *Chambers et al.* [2012]. We note that the nearest tide gauge records used by these authors were from sites located more than 3000 km from our study area, and as the authors point out, the spatiotemporal extent of the sea-level dataset needs to be enhanced before we can better understand the spatial dependence of these oscillations.

In this section, we consider the following questions: what might be the implications if we have overcorrected for 20th century sea-level rise? Could this overcorrection change our conclusion that spatial changes in locking patterns cannot explain the coral observations? Would we still require a slow slip event to explain the coral observations? In order to address these questions, we draw attention to the 1966 –1981 uplift rates from site PBK in the Banyak Islands, since the coral at this site has the best temporal resolution and the smallest uncertainties; the other sites in the Banyak Islands (PLM and PUB) have larger uncertainties, so

that any model would be less sensitive to an additional independent error of 1 to 2 mm/yr from either of these sites. If, after assuming a conservative stance of applying no sea-level rise corrections for these sites, spatial changes in coupling patterns still cannot explain the PBK uplift rate and neighbouring sites on Simeulue and Nias (and that an SSE is still required to explain the displacement rates), then we can deduce that our results are not biased by the modern sea-level rise correction that we adopted in this study.

In the case of applying no sea-level rise corrections, the alternate uplift rate at site PBK would be a lower rate of +5.8 ± 2.1 mm/yr (corresponding to a 2σ confidence interval of + 3.7 to 7.9 mm/yr). At sites PLM and PUB, the displacement rates would be -0.6 ± 5.3 and 0 ± 5.3 mm/yr, respectively. At sites LBJ, SBA and MZL, the subsidence rates would be -10.2 ±1.5, -6.4 ±1.9, and -4.5 ± 3 mm/yr, respectively. If we employ models of pure backslip on the fault (where slip on the fault does not exceed the plate subduction rate), the model with the lowest WMSSR is that shown in Figure 2b (also shown in Table S3). As mentioned in the main text, this model shows the fault locked down to 30 km depth along a 90 km section under the Banyak Islands, and creeping at the plate subduction rate at depths below 30 km. This model suggests an uplift rate of + 4.8 mm/yr at site PBK. Although this model uplift rate is within the + 3.7 mm/yr lower-end estimate at site PBK (at the 2σ level), the model would not simultaneously fit the faster subsidence rates at sites LBJ and SBA, where the model uplift rates at these two sites are -7.7 and -2.5 mm/yr, respectively. Hence, it is difficult to explain the observed displacement rates with models that only include spatially variable coupling on the megathrust, even in the case of applying no sea-level rise corrections. Our considerations here suggest that the modern sea-level rise correction that we adopt in this study does not bias our results, and our conclusion holds -- that a slow slip event is required to explain the 1966 – 1981 displacement rates.

We note that the maximum model uplift rate at site PBK shown in Figure 2b is less than the maximum uplift rate suggested by trench-normal surface uplift rate profiles shown in Figure 18 of *Meltzner et al.* [2015]'s study (their figure is reproduced and modified in Figure S7a). This is because in our study we have additional constraints from sites on Simeulue and Nias. As shown in Figure S7 (and as modeled by *Meltzner et al.* [2015]), a uniform along-strike downdip limit of locking with no downdip transition zone fails to fit displacement rates at all sites simultaneously; rather, along-strike variations in the downdip limit of locking and a downdip transition zone are needed to produce satisfactory fits at all sites. Because we incorporated these modifications in our models, the maximum model uplift rate at site PBK is less than that suggested by *Meltzner et al.* [2015].

Text S3.

Instrumental catalogues of global seismicity

There are no known records of major earthquakes in the Sumatran region between 1956 and 1966, based on both the coral microatolls and historical records [*Newcomb and McCann*, 1987]. In addition, we searched the National Earthquake Information Center (NEIC) and International Seismological Centre (ISC) catalogs for M6+ earthquakes around Sumatra, from 1956 to 2004. Figure 1 shows that pre-1966 seismicity along the Sumatran subduction zone did not exceed M7, and pre-1966 earthquakes within ~ 500 km of the Banyak Islands all have magnitudes lower than ~ 6.7. On 2 April 1956, a M6.3 earthquake occurred in the vicinity of

the Banyak Islands, but any postseismic deformation would likely have been small in amplitude and short-lived.

Text S4.

Fault geometry

The dip geometry for the fault approximates trench-normal vertical cross-sections through the Slab 1.0 model [*Hayes et al*., 2012] along the Simeulue-Nias section of the megathrust, and is consistent with the depths of relocated regional seismicity beneath southeastern Simeulue [*Tilmann et al*., 2010] (Figure S10). The variable strike of the trench along this section was also incorporated into the fault geometry. The along-strike length and downdip width of the patches on the fault are 10 km and 2 km, respectively. This geometry is slightly modified from that used by *Meltzner et al.* [2015], which results in slight differences between the depths reported in this and in the earlier paper. The map-view locations of the fully locked, partially locked, and freely slipping patches should be comparable between the two papers, but the depths are only approximately comparable. The broader conclusions and implications of either paper should not be impacted by these small differences.

Coupling model parameters

For all time periods, we assigned the coupling ratio along the shallowest 22 km of the fault to 0.4. The shallow region of partial coupling is needed to explain the observed coral displacement rates in southern Simeulue and northern Nias. The location of this shallow, partially coupled zone is consistent with that of the updip seismic/aseismic transition zone reported by *Tilmann et al*. [2010]. However, we note that the shallow region of the megathrust here is capable of rupturing during large earthquakes, as suggested by the M 7.6 tsunami earthquake of 1907 [*Kanamori et al*., 2010].

In order to fit the observed subsidence rates in the Banyak Islands, we included in the models a region of partial coupling along the downdip portion of the fault (a downdip transition zone). If this downdip transition zone is not included, then either the model subsidence rates are too large to fit the data at one or more sites, or uplift, instead of subsidence, occurs at other sites (Figure S10). We tested a range of values for the updip limit, downdip limit and coupling ratio of the downdip transition zone. For the updip and downdip limits, we tested depths ranging between 30 and 70 km, which are consistent with previous regional and global studies of locking and transition zone depths [*McCaffrey et al*., 2000; *Tichelaar and Ruff*, 1993].

In addition, models with a downdip limit of the fully coupled zone that is uniform along strike yielded poor data-model fits. However, if we incorporate a deeper downdip limit of full coupling under Simeulue Island, the data-model fits improve substantially (Figure S10). Hence, we estimated separate downdip limits under Simeulue and the Banyak Islands, respectively. We successively tested downdip limits ranging from 20 to 55 km, at 5 km depth increments.

To demonstrate the trade-offs between various parameters in the coupling and SSE models, Figures S11 and S13 show how the weighted mean of sum of squared residuals (WMSSR) changes as each parameter is perturbed from the preferred, best-fit values.

Text S5.

Inverse models

We inverted the coral data to obtain an estimated slip distribution, and with this, predicted model displacements to compare with the data. Our goal here was to ensure that we had not overlooked any distribution of coupling which could explain the Banyak Islands uplift rates. In the inversion, slip was constrained to slip backwards at rates from 0 to 40 mm/yr (the full plate subduction rate). Due to the limited spatial coverage of the data (and resulting limitations in model resolution), our objective was simply to see if there is any model (even one that does not fit our expectation of smoothness) that can fit the data; if not, this helps to confirm our conclusion that backslip alone cannot explain the 1966 – 1981 coral displacement rates . We therefore designed a fault model with coarse subfault patches (50 by 50 km in size), and did not apply any Laplacian smoothing constraints to the inversion.

We performed a bounds-constrained linear least squares inversion using a priori knowledge of the full plate subduction rate of 4 cm/yr. To determine coupling models for each of the three periods, where each patch was constrained to only slip backwards, we applied a lower slip bound of 0 cm/yr of backslip and an upper slip bound of 4 cm/yr of backslip (corresponding to an uncoupled, freely slipping patch and a fully coupled patch, respectively). On the other hand, to model an SSE on the fault, we allowed both forward, thrust motion slip and backwards slip. The corresponding slip bounds applied to the inversion were: a lower bound of -4 cm/yr of backslip, and an upper bound of +4 cm/yr of backslip (corresponding to forward, thrust motion slip of 8 cm/yr, and a fully coupled patch, respectively).

Figures S14a and S14b show the inversion results for the 1981 – 2005, and 1966 – 1981 coral displacement rates, respectively. On patches with relatively good resolution (see section below), the spatial patterns of backslip in the inverse and forward models are similar to first order, although the absolute values of estimated backslip between the two models differ. Importantly, the inverse models fit the 1981 – 2005 coral displacement rates well (weighted mean of summed squared residuals = 0), while there are large misfits with the 1966 – 1981 coral displacement rates, particularly at site PBK (weighted mean of summed squared residuals = 3.1; similar to the value for the forward model in Figure 2b). Therefore, we argue that backslip alone cannot explain the 1966 – 1981 coral displacement rates.

On the other hand, if we allow for an SSE in the inverse models, i.e., we allow for thrust motion slip on the fault at rates greater than the plate subduction rate, the model displacement rates fit the 1966 – 1981 coral displacement rates significantly better (Figure S14c). However, the inverse models are sensitive to the magnitude of forward slip constraints, such that we could not confidently estimate the SSE slip rate from the inverse models.

References

Beckley, B., F. Lemoine, S. Luthcke, R. Ray, and N. Zelensky (2007), A reassessment of global and regional mean sea level trends from TOPEX and Jason-1 altimetry based on revised reference frame and orbits, *Geophysical Research Letters*, *34*(14).

Chambers, D. P., M. A. Merrifield, and R. S. Nerem (2012), Is there a 60-year oscillation in global mean sea level?, *Geophysical Research Letters*, *39*(18), n/a-n/a, doi:10.1029/2012GL052885.

Hamlington, B., R. Leben, R. Nerem, W. Han, and K. Y. Kim (2011), Reconstructing sea level using cyclostationary empirical orthogonal functions, *Journal of Geophysical Research: Oceans (1978–2012)*, *116*(C12).

Hayes, G. P., D. J. Wald, and R. L. Johnson (2012), Slab1.0: A three-dimensional model of global subduction zone geometries, *Journal of Geophysical Research: Solid Earth*, *117*(B1), B01302, doi:10.1029/2011JB008524.

Jevrejeva, S., A. Grinsted, J. Moore, and S. Holgate (2006), Nonlinear trends and multiyear cycles in sea level records, *Journal of Geophysical Research: Oceans (1978–2012)*, *111*(C9).

McNeill, L. C., and T. J. Henstock (2014), Forearc structure and morphology along the Sumatra-Andaman subduction zone, *Tectonics*, *33*(2), 2012TC003264, doi:10.1002/2012TC003264.

Meltzner, A. J., K. Sieh, H.-W. Chiang, C.-C. Shen, B. W. Suwargadi, D. H. Natawidjaja, B. Philibosian, and R. W. Briggs (2012), Persistent termini of 2004- and 2005-like ruptures of the Sunda megathrust, *Journal of Geophysical Research: Solid Earth*, *117*(B4), B04405, doi:10.1029/2011JB008888.

Meltzner, A. J., et al. (2015), Time-varying interseismic strain rates and similar seismic ruptures on the Nias-Simeulue patch of the Sunda megathrust, *Quaternary Science Reviews*, doi:10.1016/j.quascirev.2015.06.003, in press.

Newcomb, K. R., and W. R. McCann (1987), Seismic history and seismotectonics of the Sunda Arc, *Journal of Geophysical Research: Solid Earth*, *92*(B1), 421-439, doi:10.1029/JB092iB01p00421.

Ponte, R. M., and F. Lyard (2002), Effects of unresolved high-frequency signals in altimeter records inferred from tide gauge data, *Journal of Atmospheric and Oceanic Technology*, *19*(4), 534-539.

Tilmann, F. J., T. J. Craig, I. Grevemeyer, B. Suwargadi, H. Kopp, and E. Flueh (2010), The updip seismic/aseismic transition of the Sumatra megathrust illuminated by aftershocks of the 2004 Aceh-Andaman and 2005 Nias events, *Geophysical Journal International*, *181*(3), 1261-1274.

Woodworth, P. L., N. J. White, S. Jevrejeva, S. J. Holgate, J. A. Church, and W. R. Gehrels (2009), Evidence for the accelerations of sea level on multi-decade and century timescales, *International Journal of Climatology*, *29*(6), 777-789, doi:10.1002/joc.1771.

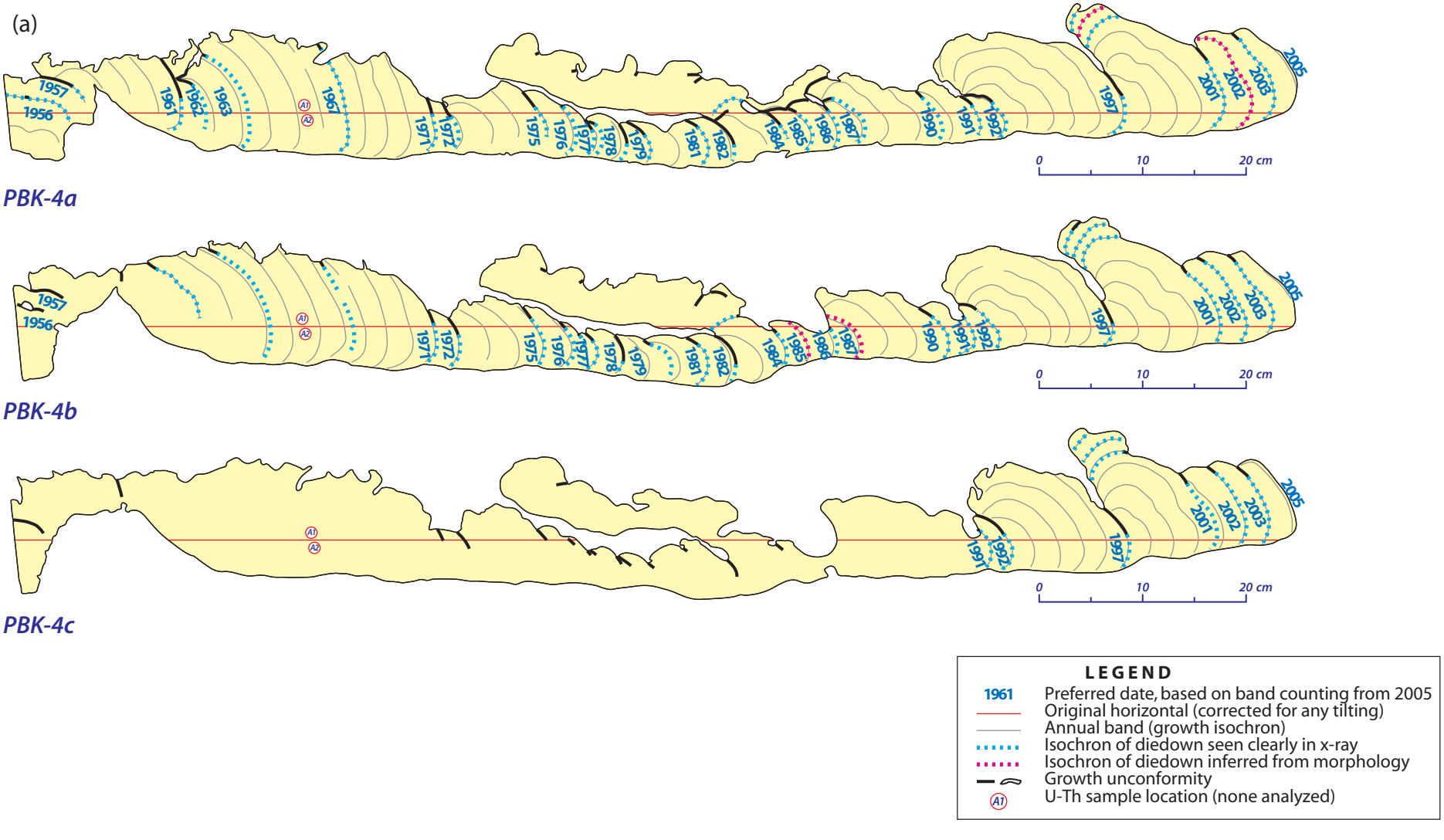

Figure S1. (a) Cross sections of slab PBK-4, from site PBK-B.

(b)

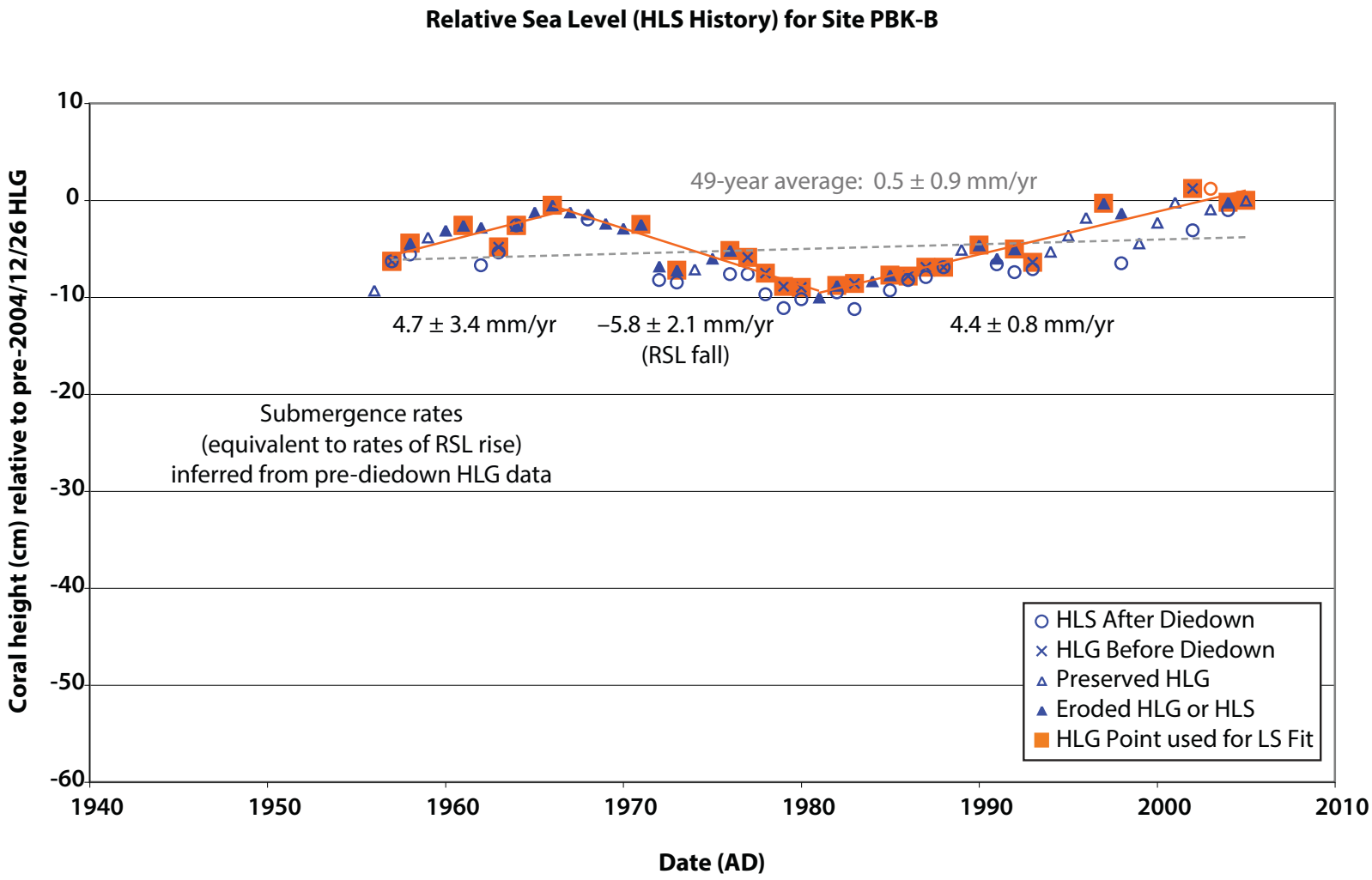

Figure S1. (b) Relative sea-level history derived from slab PBK-4.
Open orange circles above triangles designate years with inferred diedowns.

(a)

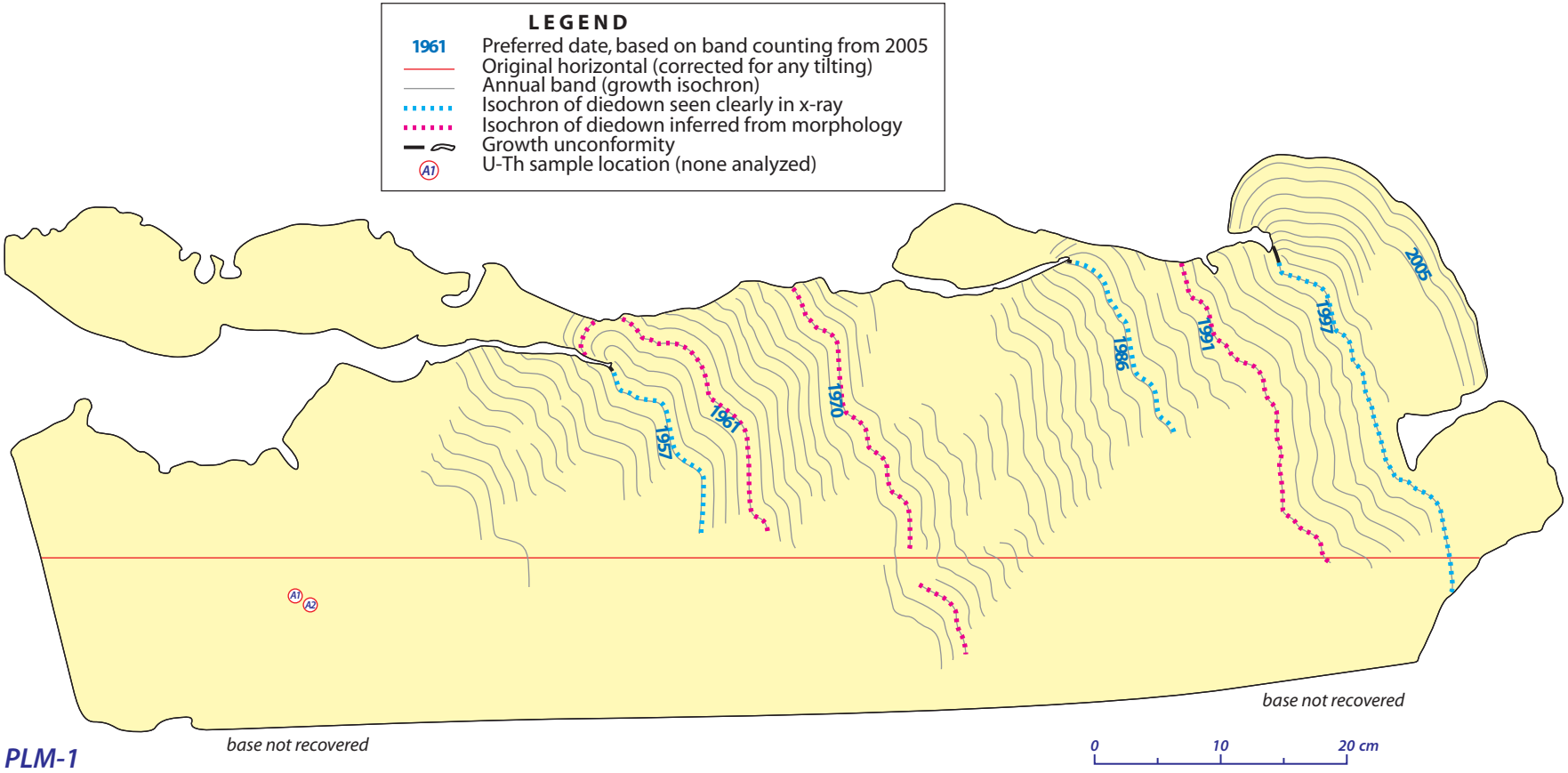

Figure S2. (a) Cross section of slab PLM-1, from site PLM-A.

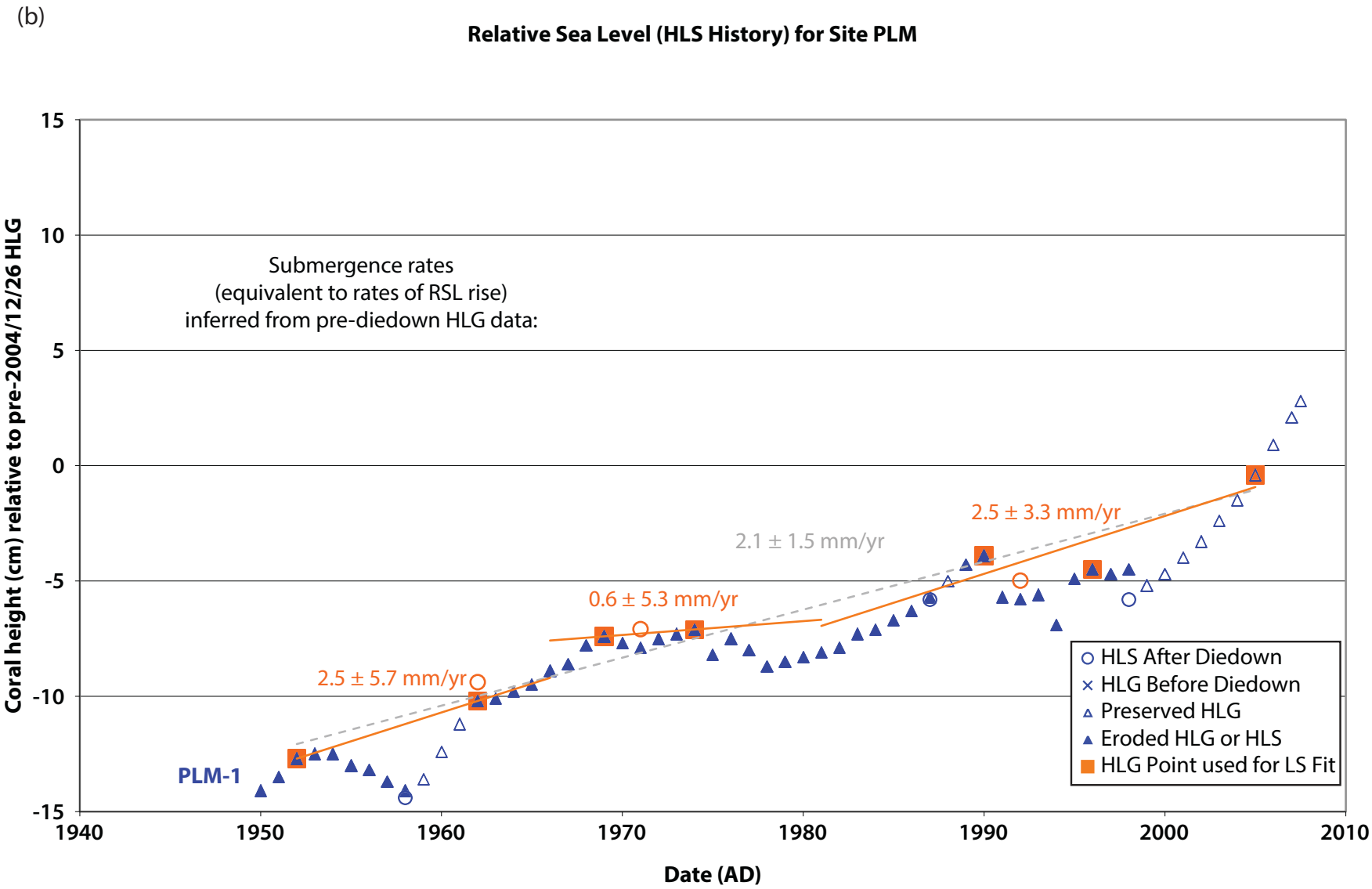

Figure S2. (b) Relative sea-level history derived from slab PLM-1.
Open orange circles above triangles designate years with inferred diedowns.

(a)

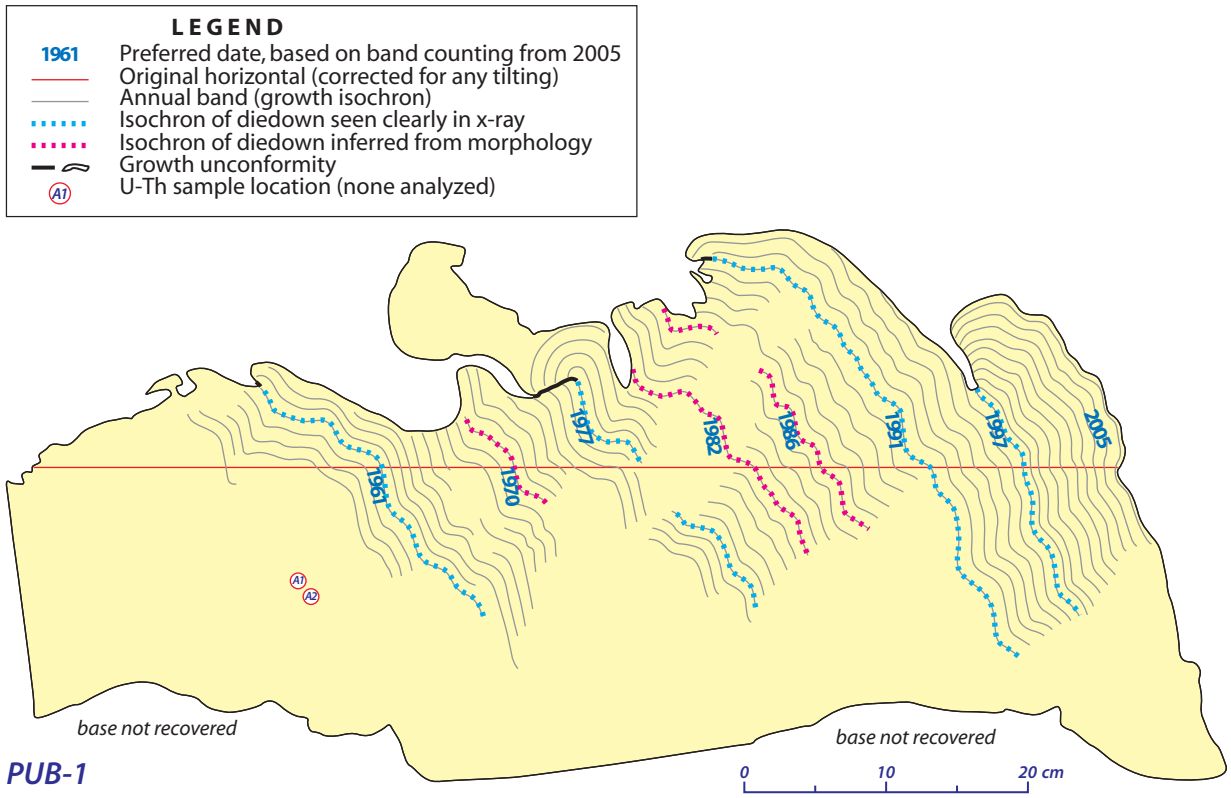

Figure S3. (a) Cross section of slab PUB-1, from site PUB-A.

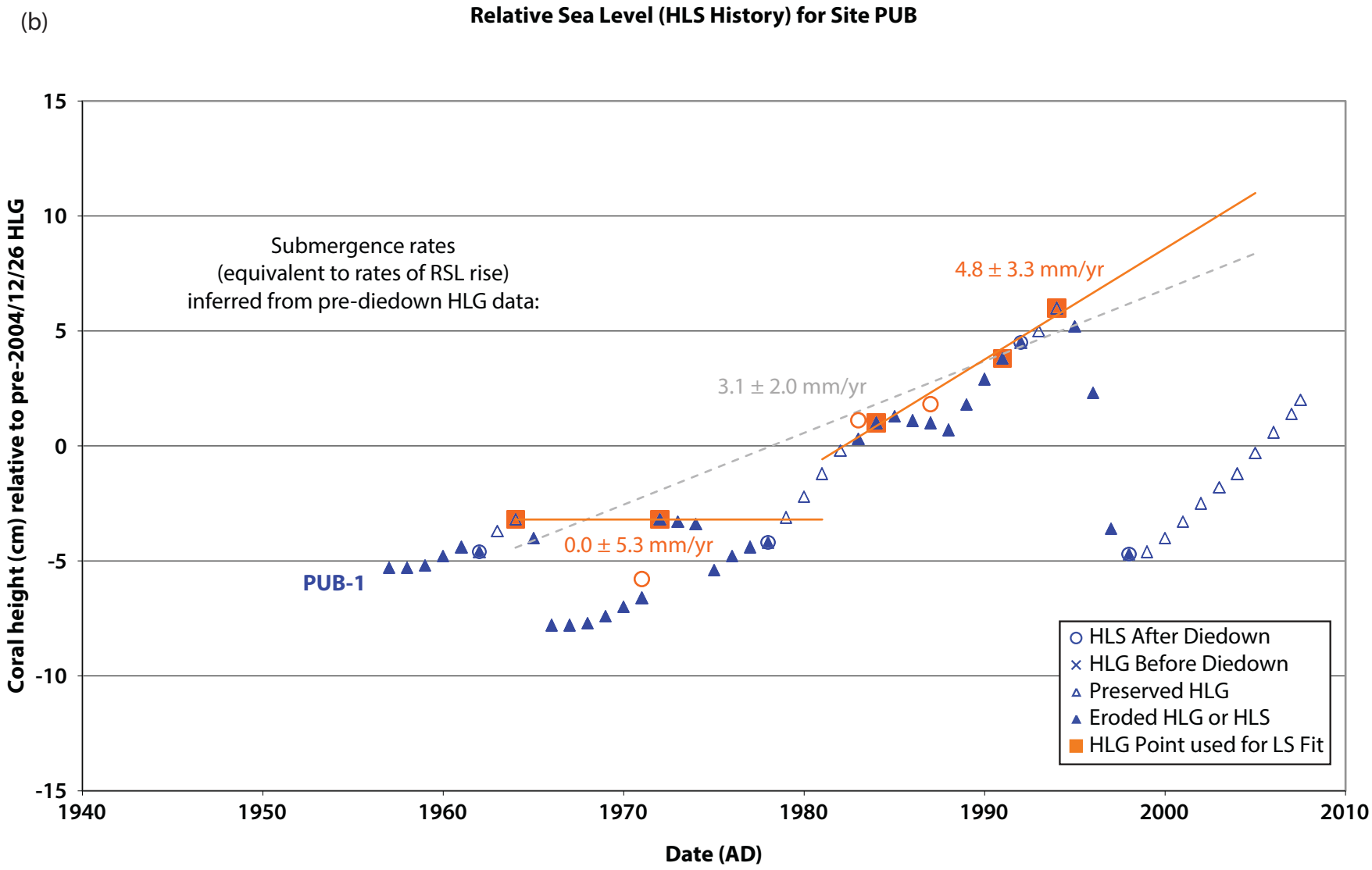

Figure S3. (b) Relative sea-level history derived from slab PUB-1.
Open orange circles above triangles designate years with inferred diedowns.

(a)

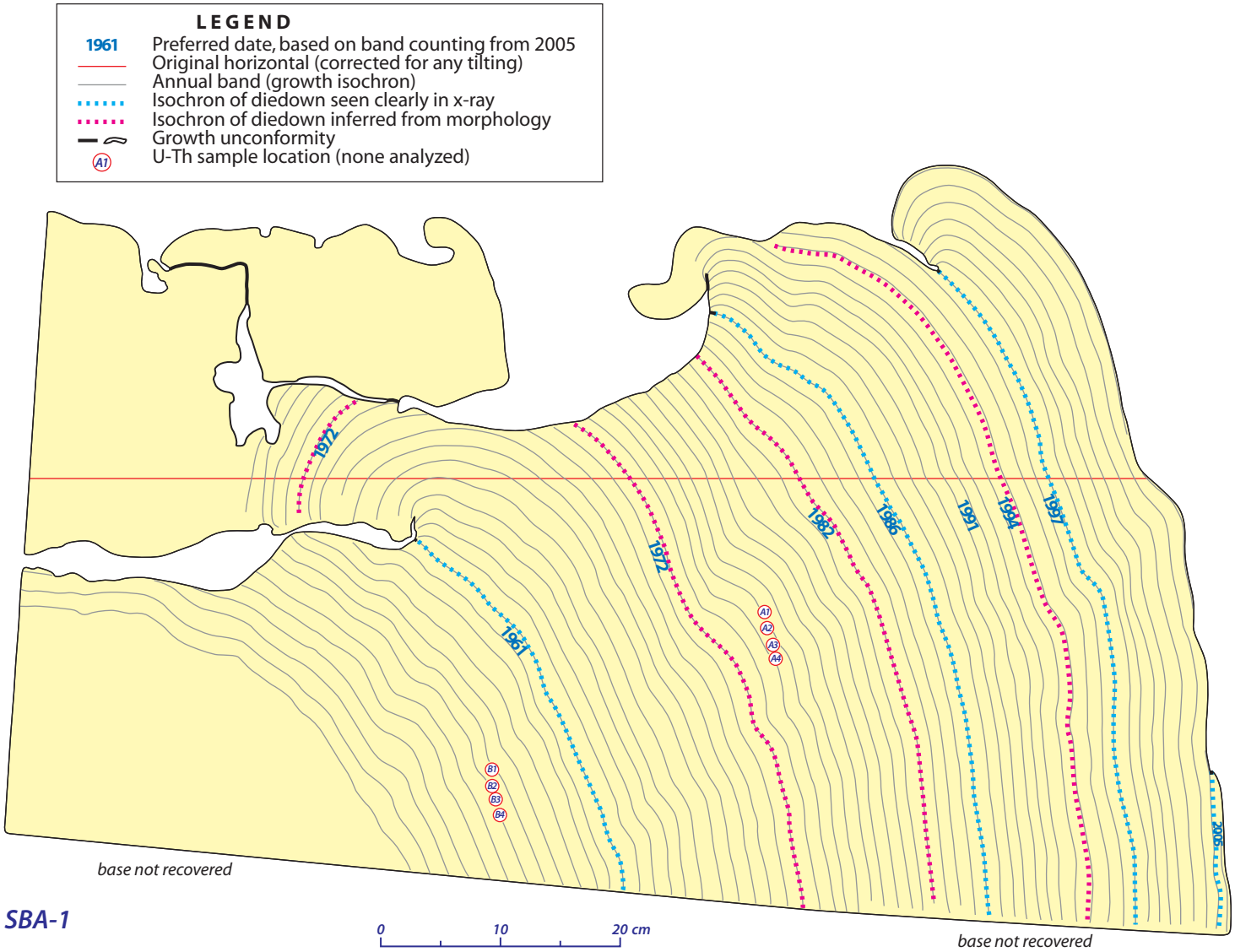

Figure S4. (a) Cross section of slab SBA-1, from site SBA-A.

(b)

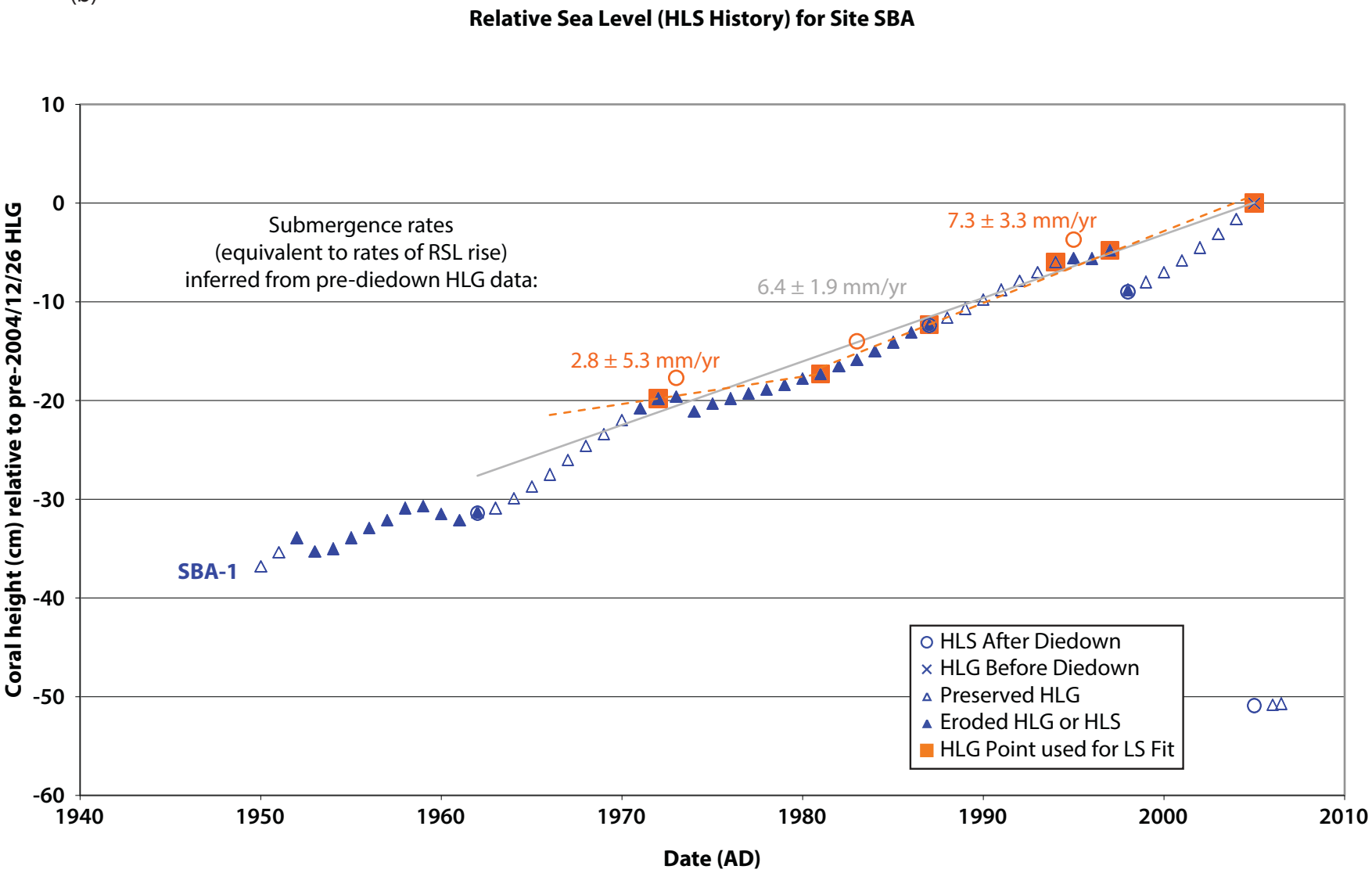

Figure S4. (b) Relative sea-level history derived from slab SBA-1.
Open orange circles above triangles designate years with inferred diedowns.

(a)

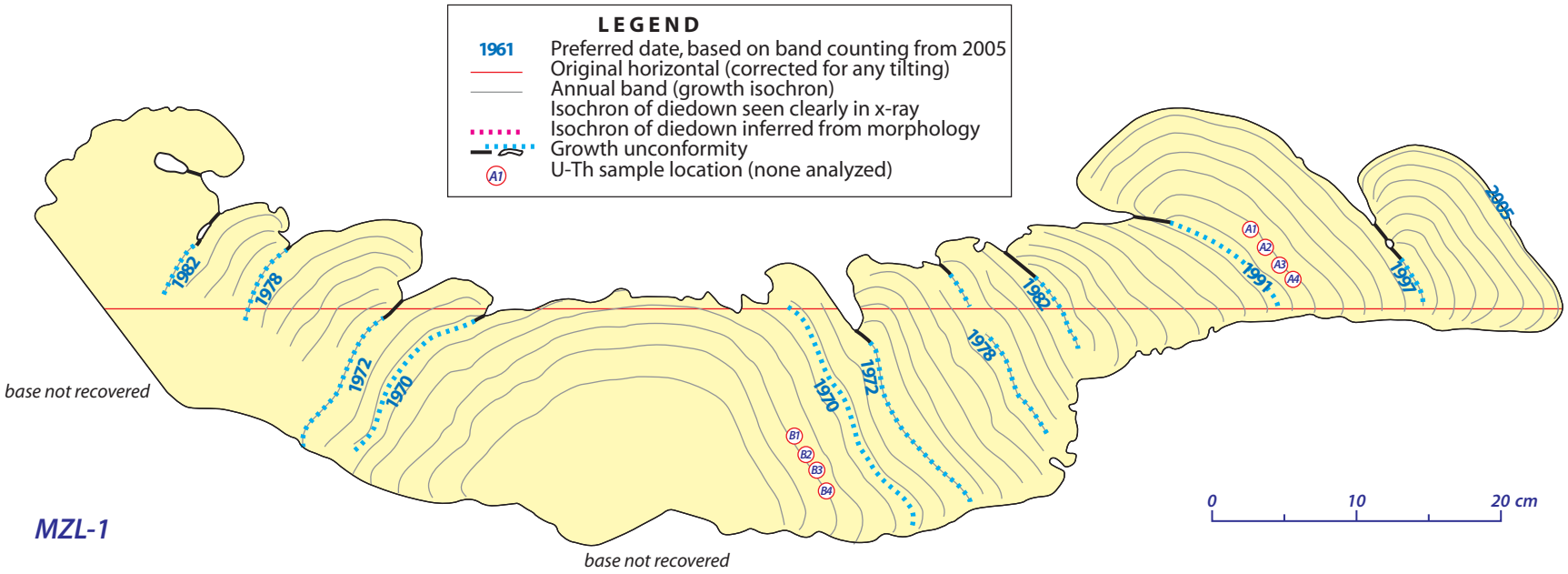

Figure S5. (a) Cross section of slab MZL-1, from site MZL-A.

(b)

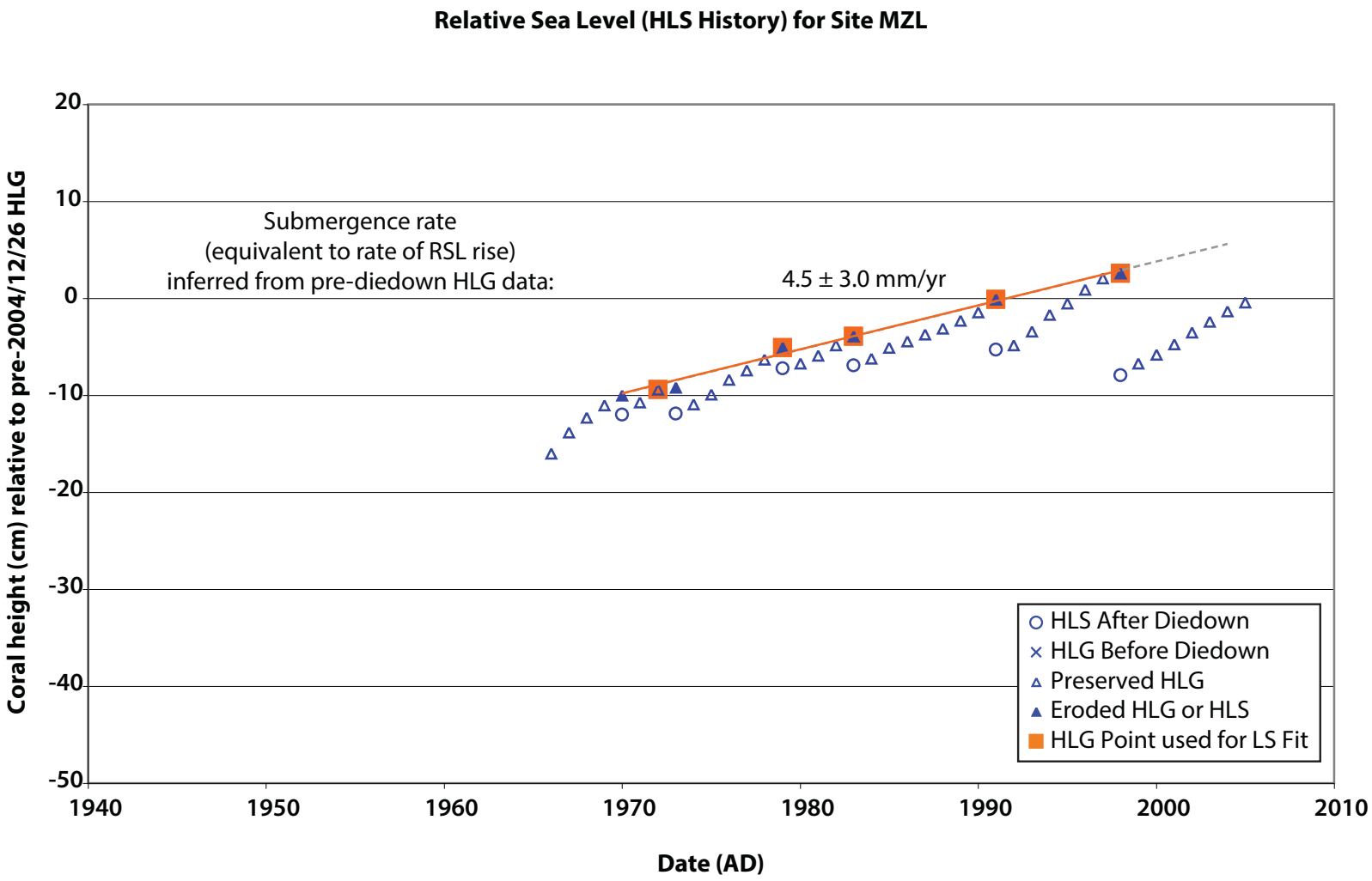

Figure S5. (b) Relative sea-level history derived from slab MZL-1.

(a)

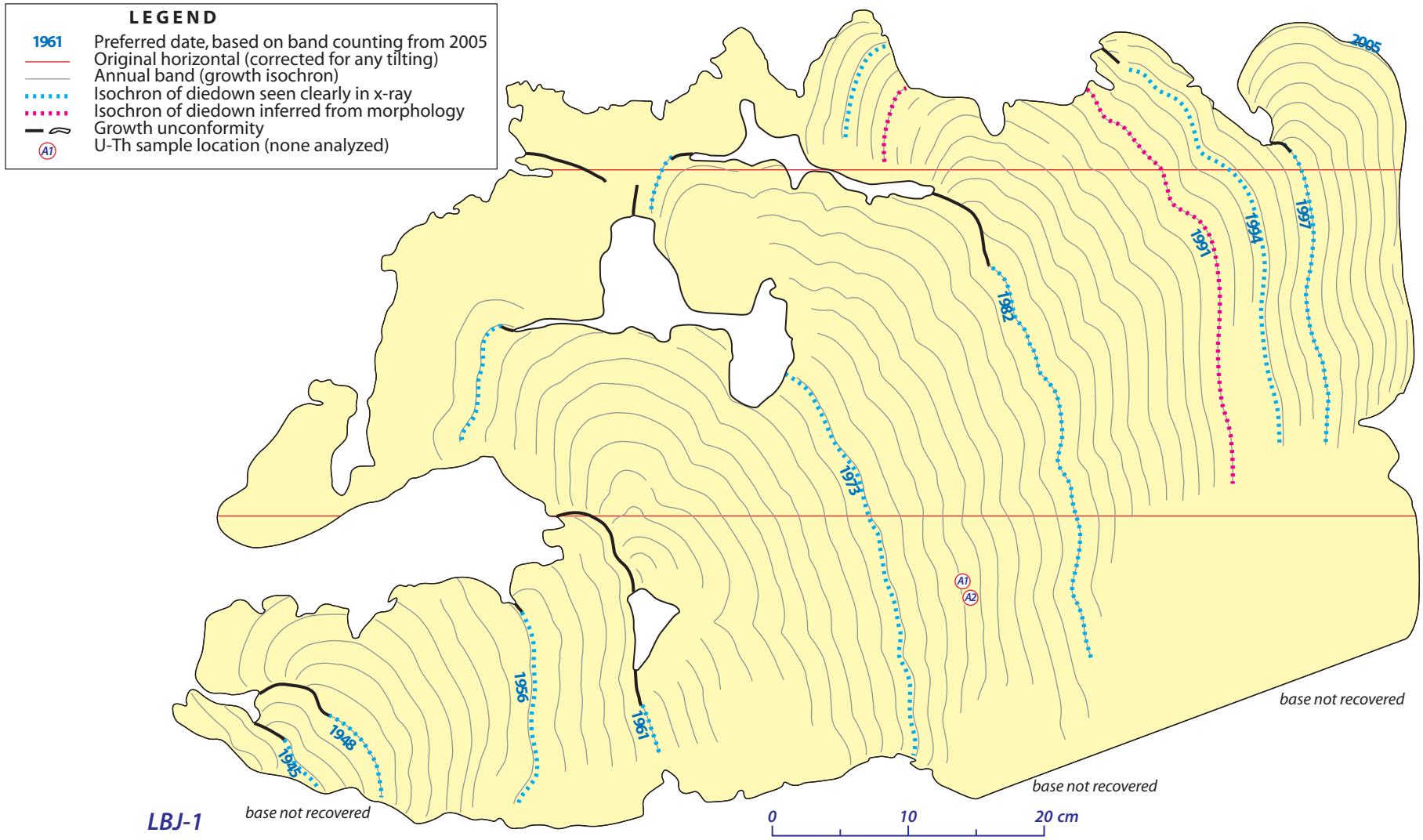

Figure S6. (a) Cross section of slab LBJ-1, from site LBJ-A.

(b)

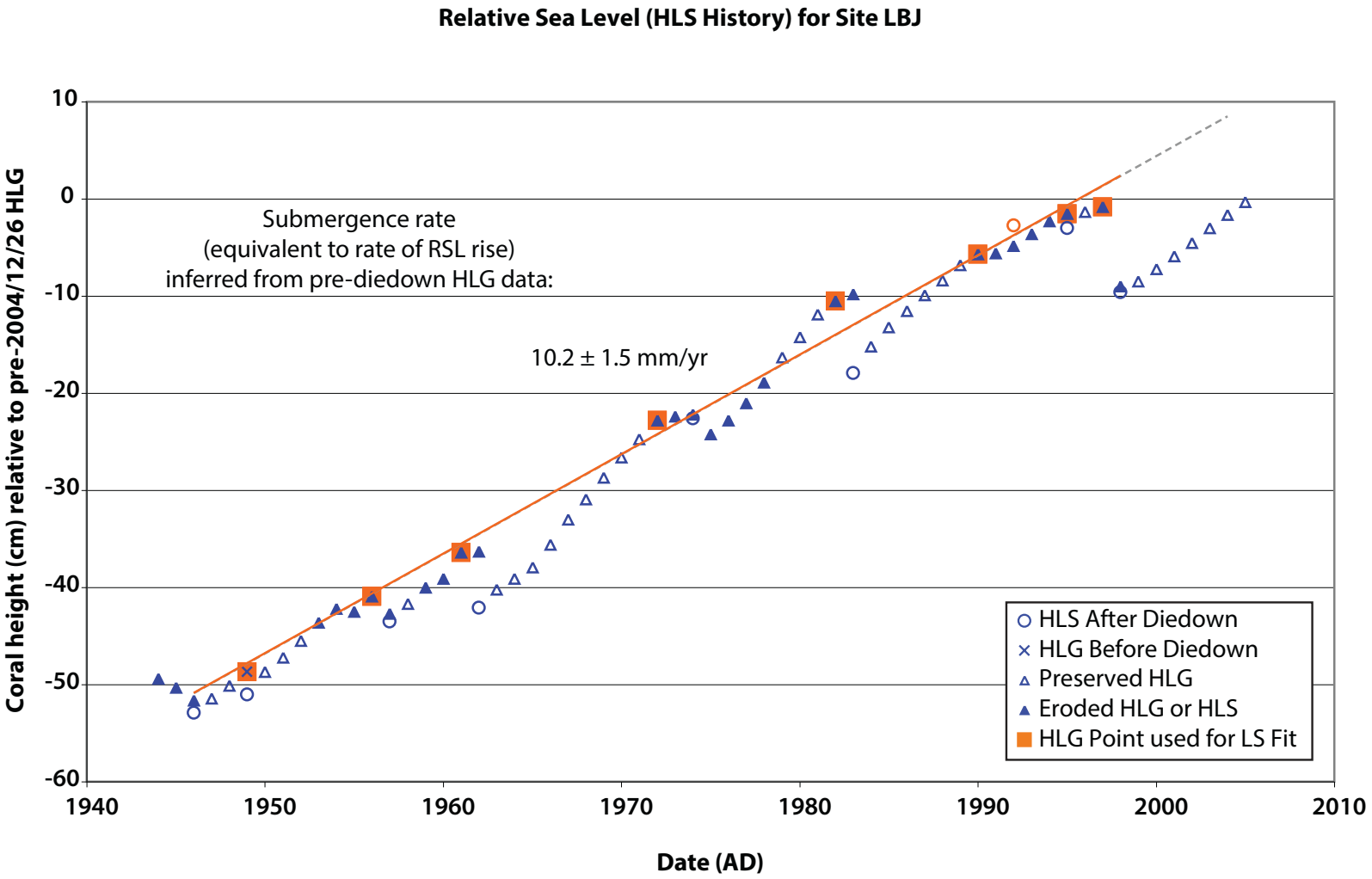

Figure S6. (b) Relative sea-level history derived from slab LBJ-1.
Open orange circles above triangles designate years with inferred diedowns.

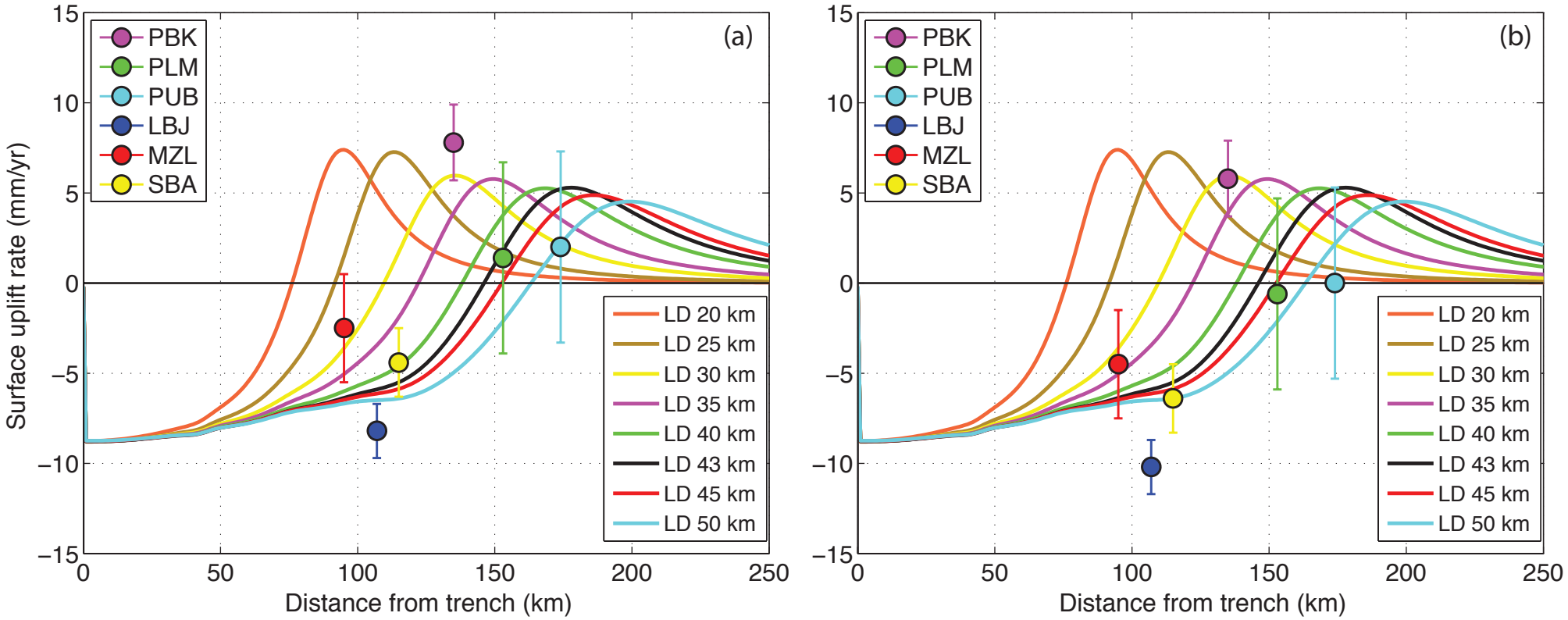

Figure S7. (a) Figure 18 from *Meltzner et al.* [2015], showing model profiles of surface uplift and subsidence, plotted as a function of distance from the trench, and for various downdip limits of locking (LD, locking depth). Superimposed are 1966 – 1981 vertical displacement rates for each site (for MZL, SBA and LBJ, the 20th century displacement rates are plotted). (b) Same model profiles shown in (a), but the 2 mm/yr modern sea level correction is removed from the 1966 – 1981 displacement rates at each site. In each case, none of the locking depth profiles can simultaneously explain displacement rates at all six sites.

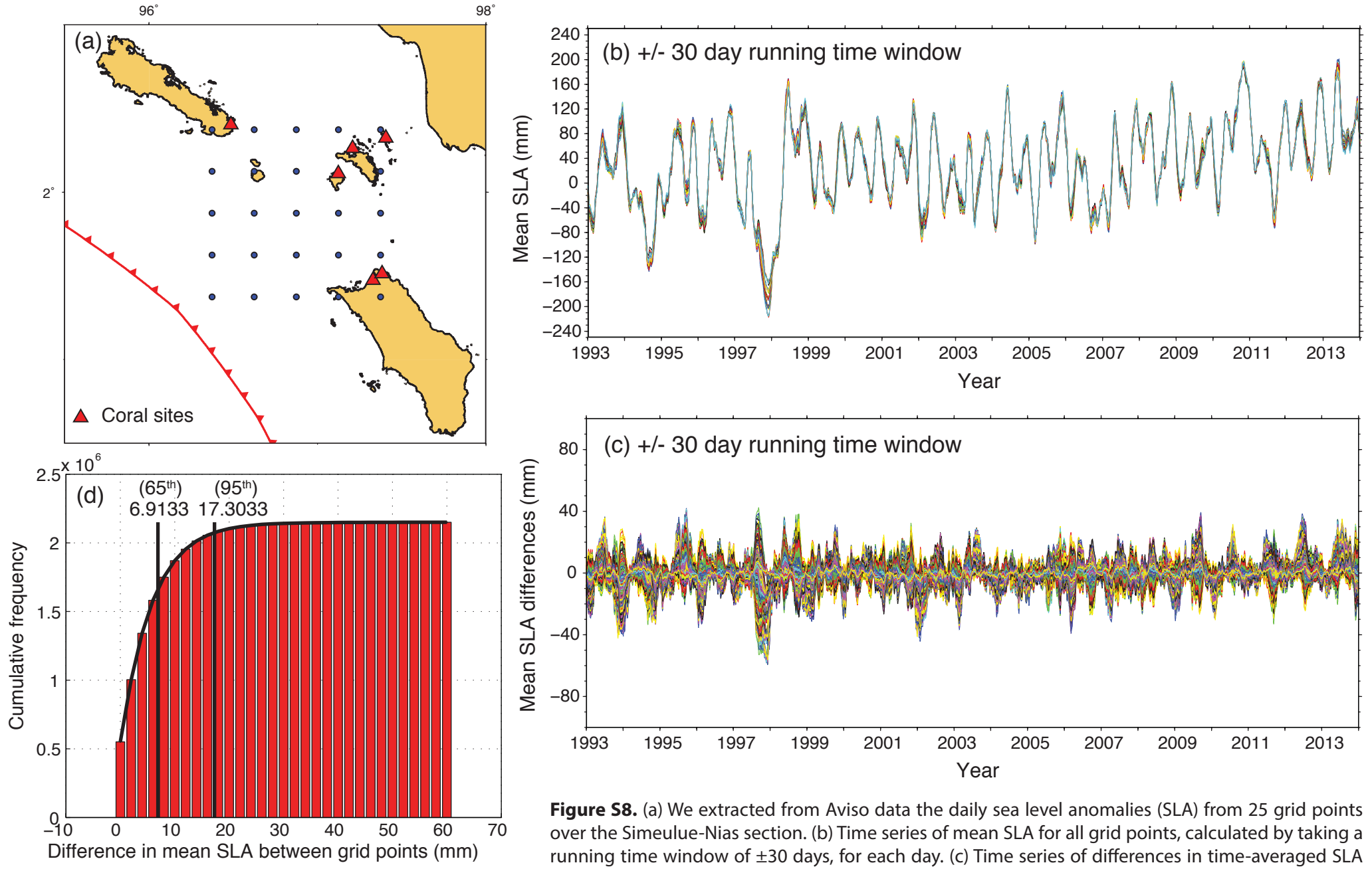

Figure S8. (a) We extracted from Aviso data the daily sea level anomalies (SLA) from 25 grid points over the Simeulue-Nias section. (b) Time series of mean SLA for all grid points, calculated by taking a running time window of ±30 days, for each day. (c) Time series of differences in time-averaged SLA between each pair of grid points. (d) Cumulative frequency histogram of mean SLA differences between each pair of grid points, and values corresponding to the 65th and 95th percentile of the data.

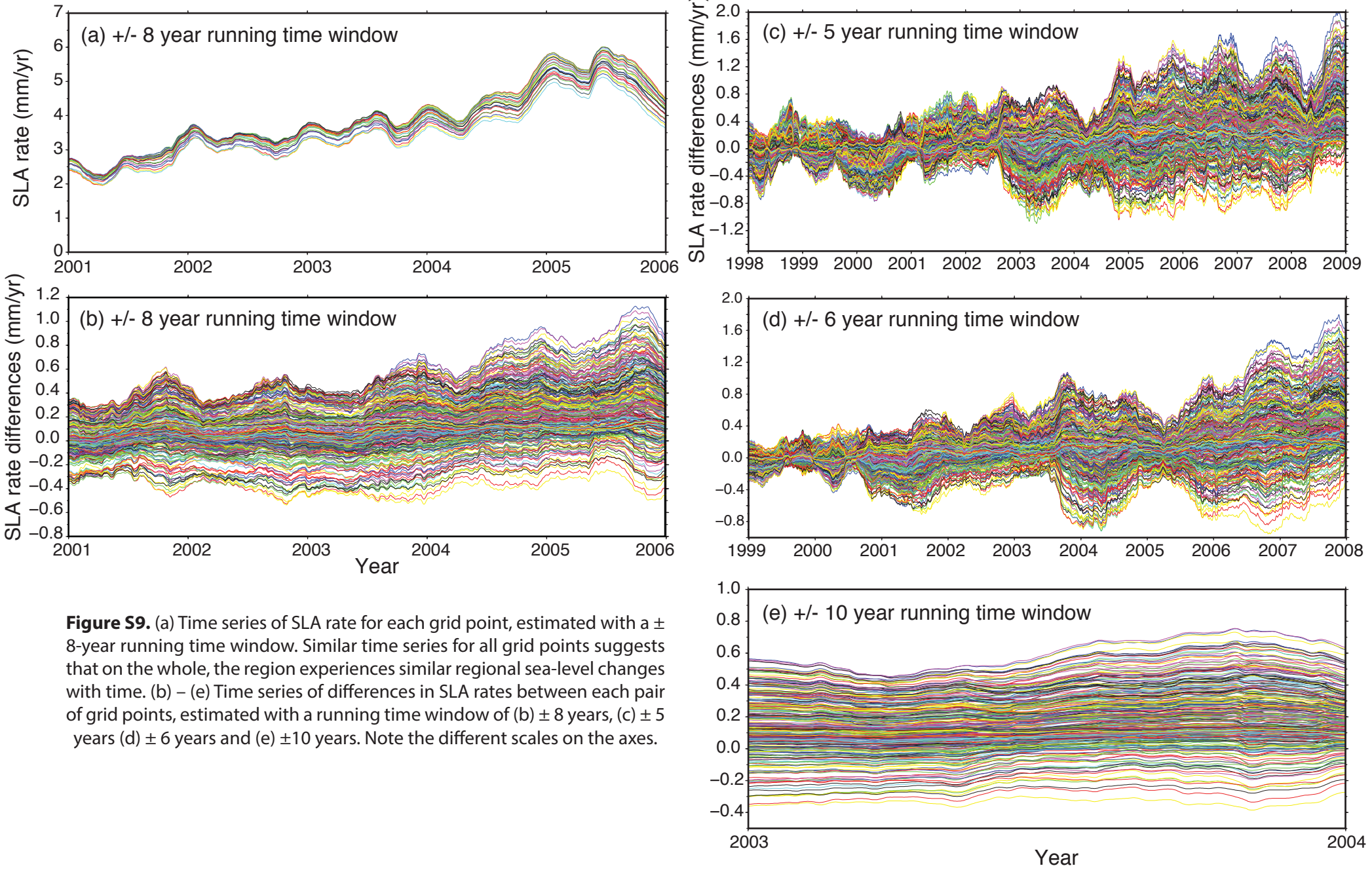

Figure S9. (a) Time series of SLA rate for each grid point, estimated with a ± 8-year running time window. Similar time series for all grid points suggests that on the whole, the region experiences similar regional sea-level changes with time. (b) – (e) Time series of differences in SLA rates between each pair of grid points, estimated with a running time window of (b) ± 8 years, (c) ± 5 years (d) ± 6 years and (e) ±10 years. Note the different scales on the axes.

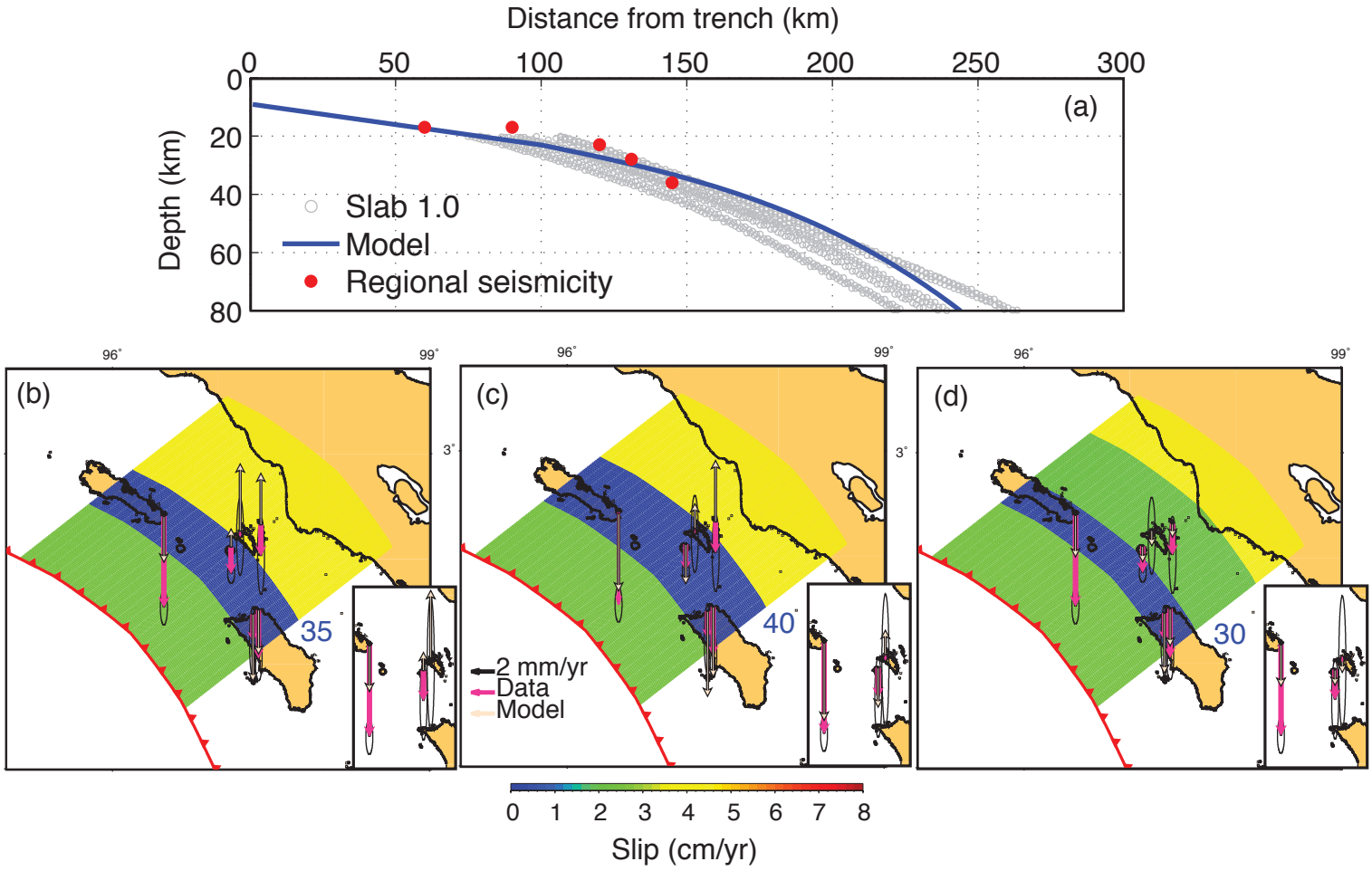

Figure S10. (a) The vertical cross-section of the fault approximates the Slab 1.0 model of *Hayes et al*. [2012] along the Simeulue-Nias section of the megathrust. Regional seismicity locations are based on *Tilmann et al.* [2010]'s results from southeastern Simeulue. (b)–(d) In the case of not including a downdip transition zone in the model (b,c), it is difficult to fit the displacement rates in the Banyak Islands within their 2σ level of uncertainties, whereas fits improve significantly with the inclusion of a downdip transition zone (d). The locking depth in each model is labeled. Data vectors in the main part of each figure correspond to 1981 – 2005 vertical displacement rates; insets show 1956 – 1966 vertical displacement rates. (b) A uniform along-strike locking depth of 35 km results in uplift, instead of subsidence, at all three Banyak Islands sites. (c) A uniform along-strike locking depth of 40 km results in too much uplift at site PUB, the site farthest from the trench. (d) Significantly better fits result from including a downdip transition zone at 30 to 60 km depths that is slipping at 50% of the plate subduction rate. However, a deeper locking depth under Simeulue Island is needed to fit the displacement rate at LBJ (as shown in our preferred best-fit model in Figure 2a).

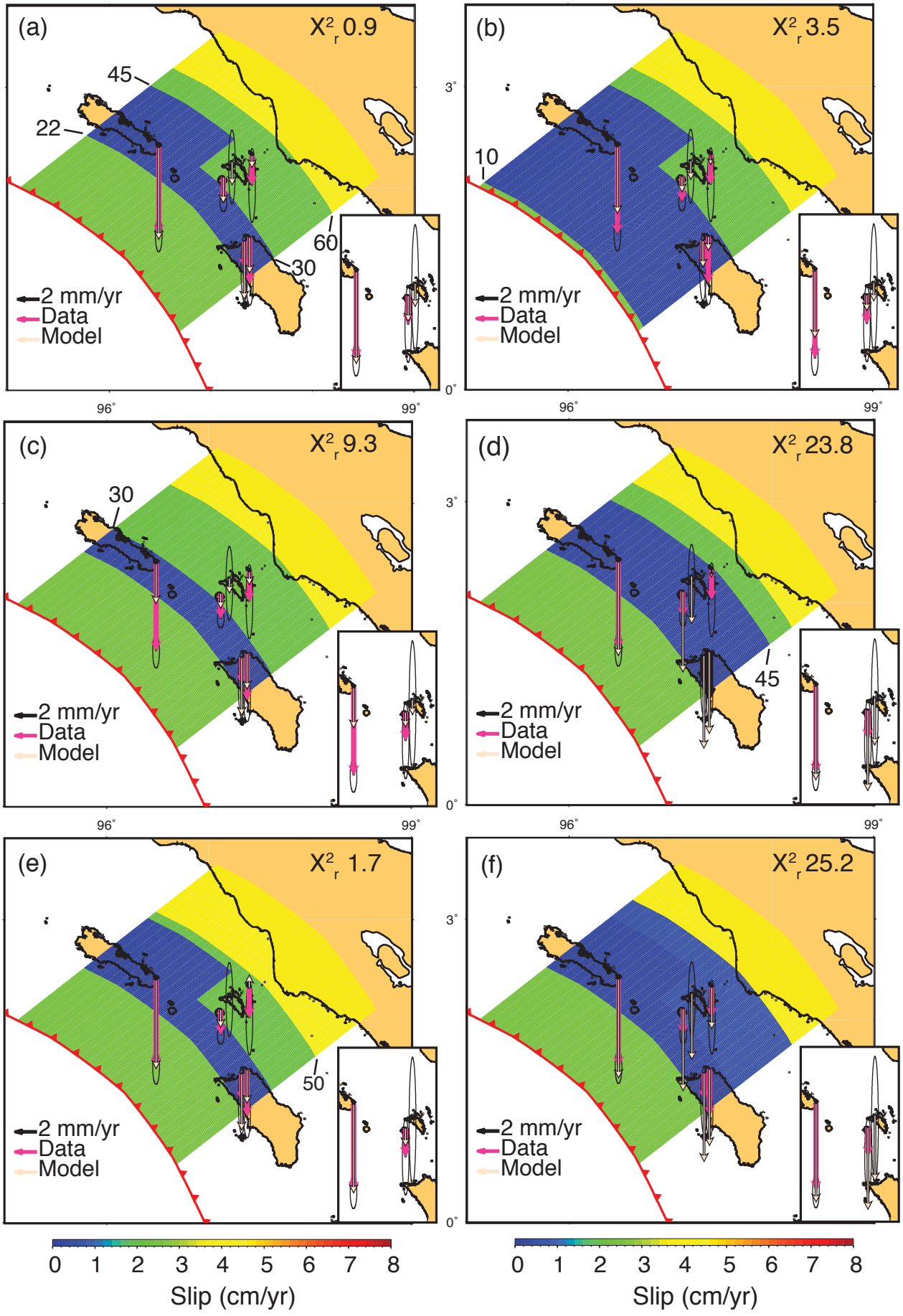
(a)
X^2_r 0.9
45
22
60
30
2 mm/yr
Data
Model
(b)
X^2_r 3.5
10
(c)
X^2_r 9.3
30
(d)
X^2_r 23.8
45
(e)
X^2_r 1.7
50
(f)
X^2_r 25.2
3°
0°
96°
99°
0 1 2 3 4 5 6 7 8
Slip (cm/yr)

Figure S11. Sensitivity of data-model fits to various backslip model parameters (data-model fits are quantified by the weighted mean of the sum of squared residuals), by changing parameters, one at a time, from those in the preferred best-fit backslip model in (a). (a) The preferred best-fit backslip model, with the updip limit of locking at 22 km depth, the downdip limit of the fully coupled zone at 30 km depth under the Banyak Islands and northern Nias, and the downdip limit of the fully coupled zone at 45 km depth under southern Simeulue. The maximum depth of the downdip transition zone is at 60 km depth. (b) – (f) Example models with a single parameter perturbed in each case from the preferred model: (b) changing the updip limit of locking from 22 km to 10 km, (c) changing the downdip limit of the fully coupled zone along the northern part of the fault from 45 km to 30 km depth, (d) changing the downdip limit of the fully coupled zone along the southern part of the fault from 30 km to 45 km depth, (e) changing the maximum depth of the downdip transition zone from 60 km to 50 km depth, and (f) changing the coupling ratio of the downdip transition zone from 50% to 90% of the full plate subduction rate (where the full plate subduction rate is 40 mm/yr). These are only a subset of all the models considered; see Table S3 for a complete set.

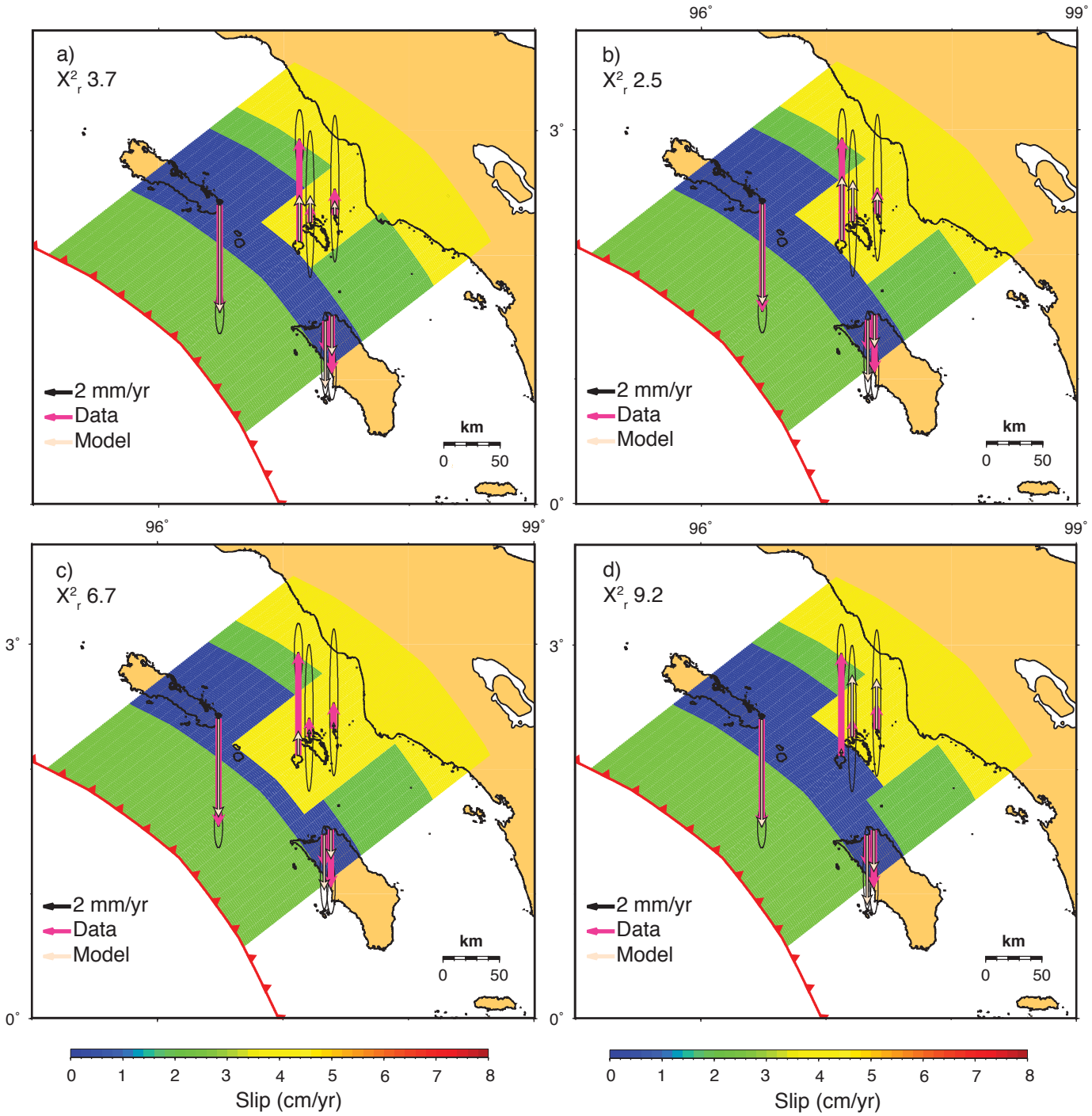

Figure S12. Additional models of spatially variable interseismic coupling that attempt to produce best fits to the 1966 – 1981 coral displacement rates. In (a), we show the same along strike location of the freely slipping patch as our preferred SSE event model (Figure 2c), with the updip limit of the freely slipping patch at 30 km depth. This fails to reproduce rapid uplift at site PBK. In (b), we widen the area of the freely slipping patch under the Banyak Islands from that shown in (a). This model produces better fits than in (a), but still fails to fit the rapid uplift rate at site PBK. This model is also shown in Figure 2b. In (c) and (d), we made further modifications to the model, but they resulted in degraded fits. Other variations that we considered are shown in Table S4.

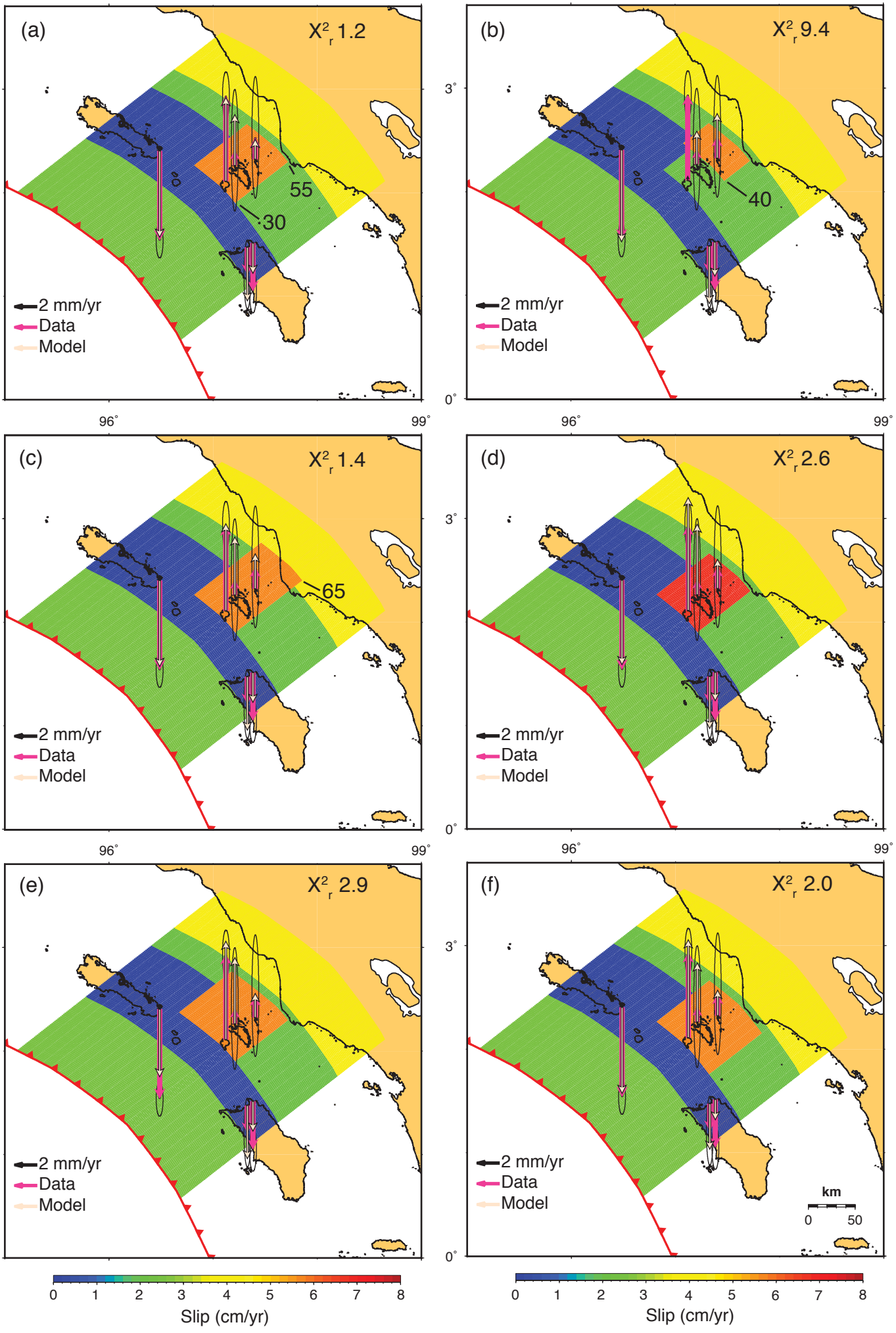
(a)
X^2_r 1.2
55
30
2 mm/yr
Data
Model
(b)
X^2_r 9.4
40
(c)
X^2_r 1.4
65
(d)
X^2_r 2.6
(e)
X^2_r 2.9
(f)
X^2_r 2.0
km
0 50
3°
0°
96°
99°
0 1 2 3 4 5 6 7 8
Slip (cm/yr)

Figure S13. Influence of various SSE parameters on data-model fits, as these parameters are deviated from the preferred SSE model. (a) The preferred SSE model, with the SSE occurring at 30 to 55 km depth over a 60 km section under the Banyak Islands, and slipping at 56 mm/yr. (b) – (f) Example models with a single parameter perturbed in each case from the preferred model: (b) changing the SSE upper depth from 30 km to 40 km, (c) changing the SSE lower depth from 55 km to 65 km, (d) changing the SSE slip rate from 56 mm/yr to 66 mm/yr, (e) extending the SSE in (a) 20 km further to the northwest, and (f) extending the SSE in (a) 20 km further to the southeast. Each of the changes in (b) through (f) result in a poorer fit of the model to the data. These are only a subset of all models considered; see Table S5 for a complete set.

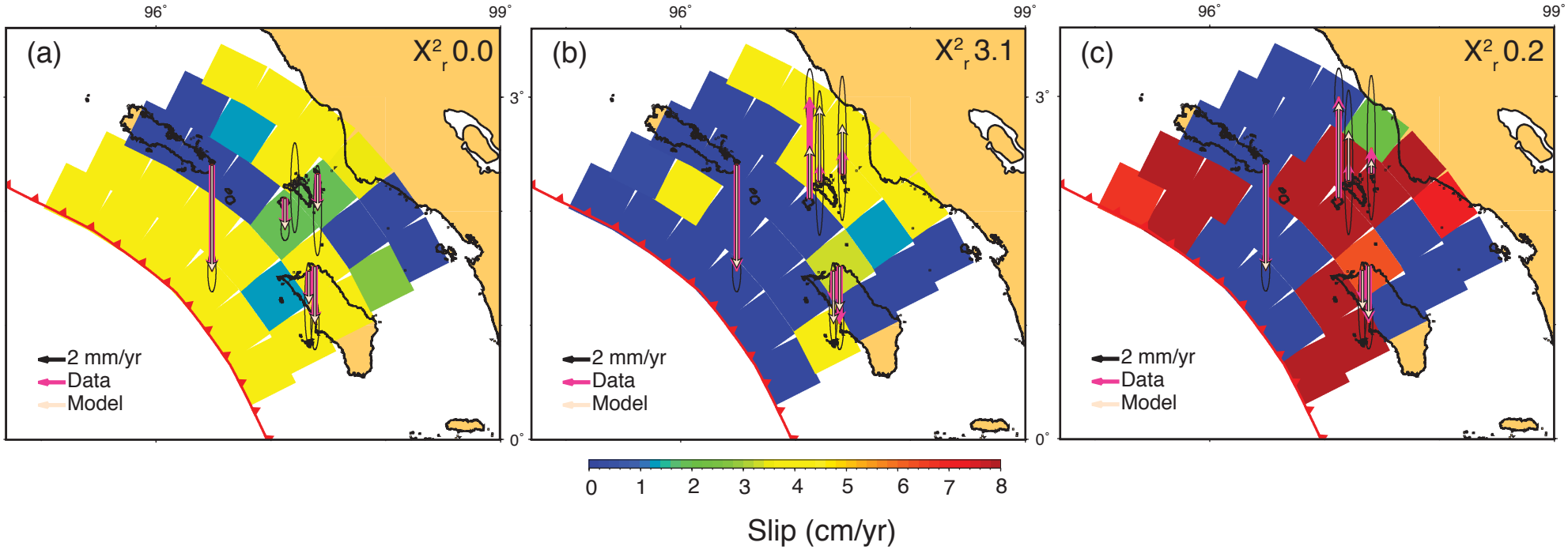

Figure S14. Inverse models for (a) the 1956 – 1966 and 1981 – 2005 coral displacement rates, assuming backward slip on the fault, (b) the 1966 – 1981 coral displacement rates, assuming backward slip on the fault, and (c) the 1966 – 1981 coral displacement rates, allowing for both forward and backward slip on the fault. Note that the color scale shows real slip values (as opposed to backslip values) to be consistent with the color scale shown in the forward models, so that a slip of 0 cm/yr indicates a locked interface, 4 cm/yr indicates a freely slipping interface (slip at the full plate subduction rate of 4 cm/yr), and slip greater than 4 cm/yr indicates slow slip at a rate greater than the full plate subduction rate.

Table S1. Coral site locations, vertical displacement rates, and 2σ level of uncertainties in rates, for each time period. For sites PBK, PLM and PUB, average vertical displacement rates for the entire time period of available data are given for reference; these rates were not used in the modeling.

Table S2. Additional uncertainties in vertical displacement rates at each site due to spatial variations in sea level, calculated by dividing the 95th percentile of mean SLA differences (17.3 mm) by the length of time over which each displacement rate was determined. The total uncertainty equals the uncertainties due to differential erosion and growth rates of the coral (calculated with the methodology of *Meltzner et al.* [2012], plus the additional uncertainty due to spatial variations in sea level. Also shown are the magnitudes of rate changes between each time period ('1966 change' is the change in rates between 1956 – 1966 and 1966 – 1981, and '1981 change' is the change in rates between 1966 – 1981 and 1981 - 2005), and their 1σ and 2σ level uncertainties.

Table S3. (a) Models of spatially variable fault coupling that yield reasonable fits to the 1956 – 1966 and 1981– 2005 displacement rates; the preferred best-fit model shown in Figure S11a is highlighted in bold. (b) Sensitivity of data-model fits to various backslip model parameters, by changing the parameters, one at a time, from those in the preferred best-fit model. A subset of these models is shown in Figure S11. (c) Testing the downdip transition zone parameters under the Banyak Islands, with a fixed downdip limit of the fully coupled zone at 45 km depth under Simeulue, an updip limit of locking at 22 km depth, and coupling ratio of 0.4 at < 22 km depths. Models that yield good data-model fits are highlighted in bold. (d) Testing the downdip limit of the fully coupled zone under Simeulue Island, starting from the subset of models highlighted in (c). (e) Testing the updip limit of locking (with a fixed coupling ratio of 0.4 at depths shallower than the updip limit), starting from the subset of models highlighted in (c). The results in (d) and (e) affirm that the four models highlighted in (c) are models that yield good data-model fits.

Table S4. Models of spatially variable fault coupling that attempt to produce best fits to the 1966 – 1981 displacement rates. (a) Testing models with different downdip limits of the fully coupled zone under the Banyak Islands, while keeping the following parameters fixed: the downdip limit of the fully coupled zone under Simeulue at 45 km depth, an updip limit of locking at 22 km depth, a coupling ratio of 0.4 at < 22 km depths, a downdip limit of the transition zone at 60 km depth, and a coupling ratio of 0.5 in the downdip transition zone. A subset of models are shown in Figure S12. (b) Testing the along-strike location of the freely slipping patch under the Banyak Islands. In each of tables, the best models are highlighted in bold.

Table S5. (a) Range of SSE models that yield good fits to the 1966 – 1981 coral displacement rates. The preferred best-fit model is highlighted in bold. (b) Sensitivity of data-model fits to various SSE model parameters, as these parameters are deviated from the preferred best-fit SSE model highlighted in (a). A subset of these models are shown in Figure S13. (c) Testing SSE depth range, slip rate, location and size. Models that yield good data-model fits are highlighted in bold.

Table S6. List of SSEs at various subduction zones, compiled by *Peng and Gomberg* [2010] and *Schwartz and Rokosky* [2007].